Electronic Supplementary Material (ESI) for ChemComm.

Electronic Supplementary Information

Confinement effects of a crystalline sponge on ferrocene and ferrocene carboxaldehyde

Gabriel Brunet,[a] Damir A. Safin,[a,b] Koen Robeyns,[b] Glenn A. Facey,[a] Ilia Korobkov,[a] Yaroslav Filinchuk,[b] and Muralee Murugesu*[a]

[a] Department of Chemstry and Biomolecular Sciences, University of Ottawa, 10 Marie Curie, Ottawa, ON, Canada, K1N 6N5.

[b] Institute of Condensed Matter and Nanosciences, MOST – Inorganic Chemistry, Université catholique de Louvain, Place L. Pasteur 1, 1348 Louvain-la-Neuve, Belgium.

*m.murugesu@uottawa.ca

Methods

General considerations

All manipulations were performed under aerobic conditions using materials as received from commercial suppliers (Sigma Aldrich, Strem Chemical). The ligand 2,4,6-tris(4-pyridyl)-1,3,5-triazine (TPT),[1] and parent MOFs **1a** and **1b**[2] were prepared according to previously published procedures.

Synthesis of 2a and 2b

As-synthesized single-crystals of **1a** and **1b** initially contain nitrobenzene in the void space of the lattice, and according to previous work, such molecules would prevent the diffusion of target guest compounds into the pores owing to the strong $\pi\cdots\pi$ interactions between the nitrobenzene solvent molecules and the triazine-based ligand.[3] The exchange of nitrobenzene by cyclohexane is therefore recommended, however, it was found that this additional step was unnecessary for the inclusion of ferrocene and ferrocene carboxaldehyde. The nitrobenzene solution can be carefully decanted, in a manner to keep the crystals in solution, and replaced by a solution of ferrocene (50 mg, 0.27 mmol) in cyclohexane (5 mL). The resulting mixture is heated to 50 ^{o}C over a period of one week in a capped vial. Successful inclusion can be identified by a change in color of the crystals from colorless to dark-brown, while maintaining their crystallinity, allowing for suitable diffraction data to be obtained on a conventional laboratory diffractometer.

2a: Selected IR: 3050 (w), 1617 (m), 1574 (m), 1514 (s), 1421 (m), 1372 (s), 1314 (m), 1212 (m), 1099 (w), 1058 (s), 1025 (s), 868 (m), 803 (s), 751 (m), 733 (m), 668 (s), 655 (s) cm^{-1}. NMR ^{1}H (DMSO-d_6, 400 MHz): δ 4.11 (s, ferrocene), 7.65 (d, $PhNO_2$), 7.82 (t, $PhNO_2$), 8.21 (d, $PhNO_2$), 8.62 (d, TPT), 8.92 (d, TPT) ppm.

2b: Selected IR: 3055 (w), 1622 (m), 1576 (m), 1514 (s), 1421 (m), 1372 (s), 1314 (m), 1212 (m), 1100 (w), 1058 (s), 1024 (s), 868 (m), 803 (s), 751 (m), 733 (m), 669 (s), 655 (s) cm^{-1}. NMR ^{1}H (DMSO-d_6, 400 MHz): δ 4.12 (s, ferrocene), 7.64 (d, $PhNO_2$), 7.82 (t, $PhNO_2$), 8.21 (d, $PhNO_2$), 8.63 (d, TPT), 8.92 (d, TPT) ppm.

Synthesis of 3

The same procedure was replicated for **3** as in **2a**/**2b**, except ferrocene carboxaldehyde (58 mg, 0.27 mmol) was dissolved in a mixture of benzene (2.5 mL) and cyclohexane (2.5 mL). Selected IR: 3066 (w), 1661 (w), 1618 (w), 1575 (w), 1575 (w), 1514 (s), 1422 (w), 1373 (m), 1343 (s), 1316 (m), 1214 (w), 1107 (w), 1059 (m), 1025 (m), 850 (m), 804 (s), 704 (s), 666 (w), 655 (s), 621

(w) cm^{-1}. NMR ^1H (DMSO-d_6, 400 MHz): δ 4.25 (m, FcCHO), 4.55 (t, FcCHO), 4.75 (d, FcCHO), 7.37 (s, benzene), 8.63 (d, TPT), 8.92 (d, TPT), 9.96 (s, FcCHO) ppm.

Measurements

Single crystal X-ray diffraction

*Compound **2a***

Single crystal X-ray diffraction data for **2a** were collected at 200(2) K on a Bruker-AXS KAPPA diffractometer equipped with a sealed Mo tube source (λ = 0.71073 Å) APEX II CCD detector. Data collection and processing were performed with the Bruker APEX II software package.[4] The structures were solved by direct methods and refined with full-matrix least-squares procedures using SHELXL.[5] All non-hydrogen atoms were refined anisotropically. The positions of the hydrogen atoms were calculated based on the geometry of related non-hydrogen atoms.

*Compounds **2b** and **3***

Diffraction data for **2b** and **3** were collected on a Mar345 image plate using MoKα radiation (λ = 0.71073 Å, Rigaku UltraX 18S, Xenocs Fox3d mirrors). Prior to the X-ray experiments the crystals were flash-cooled to 150K in a N_2 gas flow. Data integration was performed by CrysalisPro[6] and the implemented absorption correction was applied. The structures were solved by direct methods SHELXS-97[5] and refined by full-matrix least-squares procedures using SHELXL2014[5]. All non-hydrogen atoms were refined anisotropically and H atoms were placed at calculated positions and allowed to ride on the parent atoms with Ueq values 1.2 times higher than these parent atoms.

Solid-state NMR spectroscopy

Solid state ^{13}C CPMAS NMR spectra were collected on a Bruker AVANCE III 200 NMR spectrometer using a 7 mm CPMAS probe operating at a spinning speed of 4.5 kHz. The ^1H 90° pulse was 4.9 µsec. A contact time of 2 msec was used. In the case of pure crystalline ferrocene, spectra were collected with 32 scans. The ^1H T_1 relaxation time was quite long making a 60 sec recycle delay necessary. The spectra of complex **2a** were collected with 1400 scans. The ^1H T_1's were much shorter allowing a 2 sec recycle delay to be used.

Solution-state NMR spectroscopy

^1H NMR of the digested samples were conducted on a Bruker Avance 400 MHz spectrometer equipped with an automatic sample holder and a 5 mm auto tuning broadband probe with Z gradient.

Infrared spectroscopy

IR spectra were collected on all samples in the solid state on a Varian 640 FT-IR spectrometer in the 525–4000 cm^{-1} range**.**

Diffuse reflectance spectroscopy

Diffuse-reflectance spectra were measured with a Varian Cary-100 spectrophotometer using polytetrafluoroethylene (PTFE) as a reference. Kubelka-Munk spectra were normalized to allow meaningful comparisons.

Solid-state luminescence

Fluorescence spectra were recorded using a Perkin Elmer LS-50 Luminescence spectrometer equipped with a Xenon lamp and a variable angle front-surface accessory. Solid samples were sandwiched between two quartz disks.

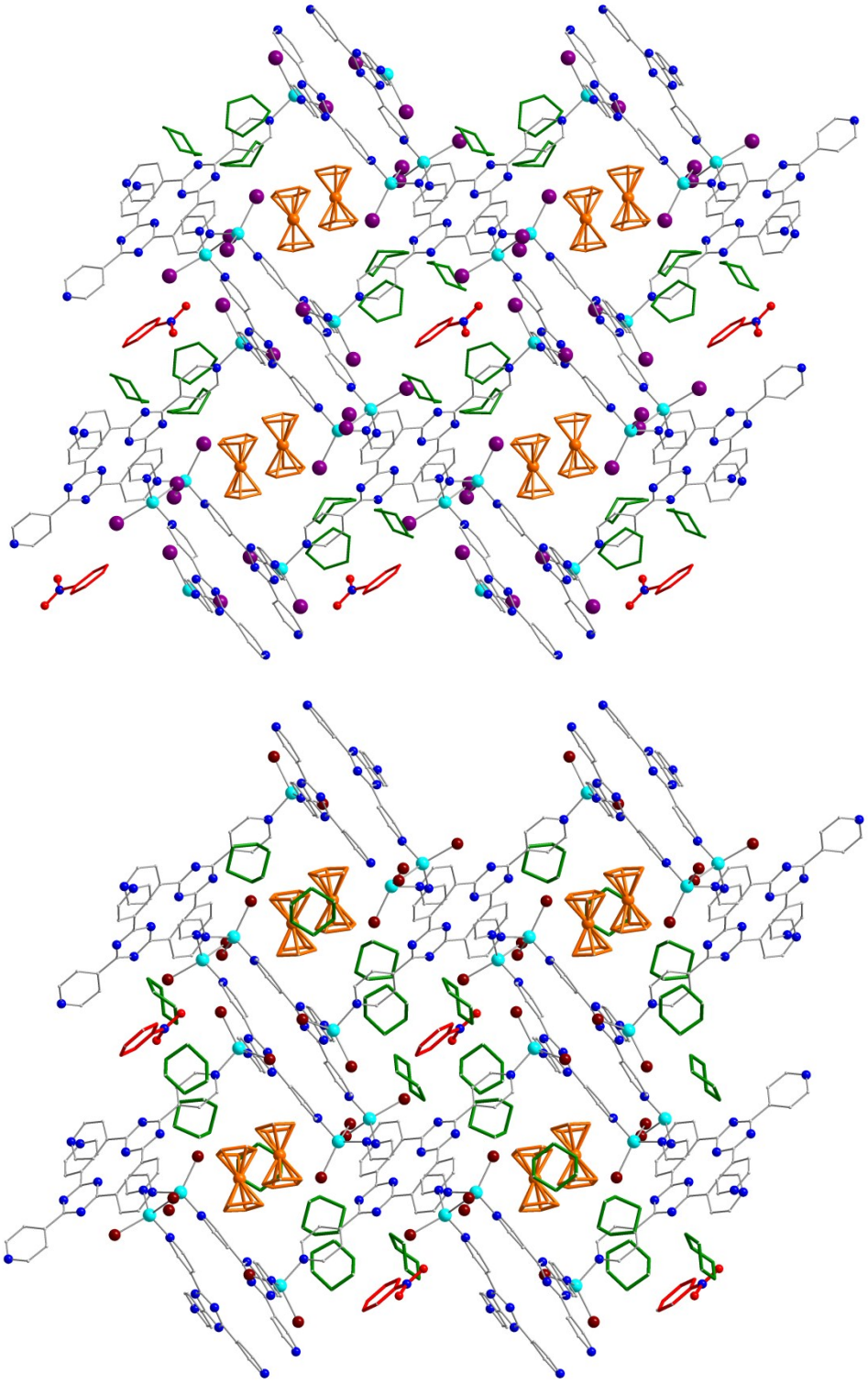

Fig. S1 Packing arrangement of **2a** (top) and **2b** (bottom) along the *b*-axis, depicting the ferrocene guests (orange), and the nitrobenzene (red) and cyclohexane (green) solvent molecules. Hydrogen atoms and positional disorder are omitted for clarity.

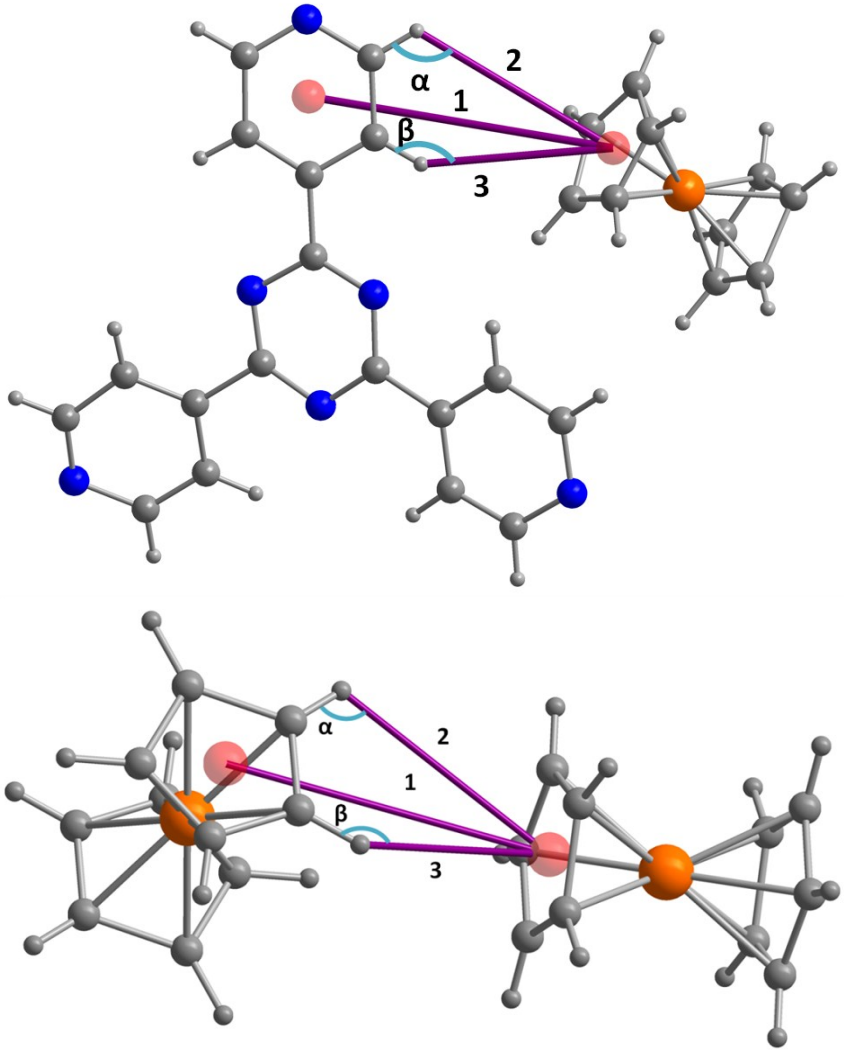

Fig. S2 Representative $\pi\cdots\pi$ interactions between the ferrocene molecules and the host framework found in **2a** and **2b** (top), and analogous interactions found in the structure of pure ferrocene (bottom).

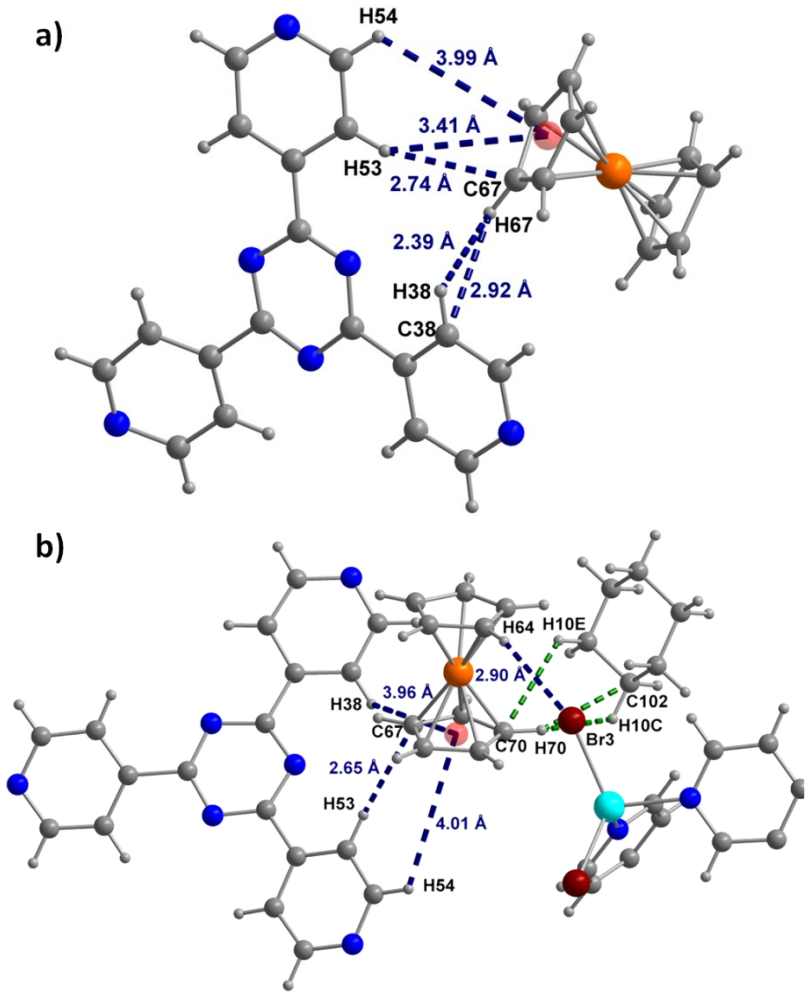

Fig. S3 Host-guest interactions of **2a** and **2b**. Offset y-shaped interactions of ferrocene in **2a** (a) and **2b** (b). Host-guest interactions are shown in blue, while guest-solvent interactions are displayed in green. Cp ring centroids are displayed as red spheres. Colour code: orange (Fe), blue (N), maroon (Br), cyan (Zn), gray (C), white (H).

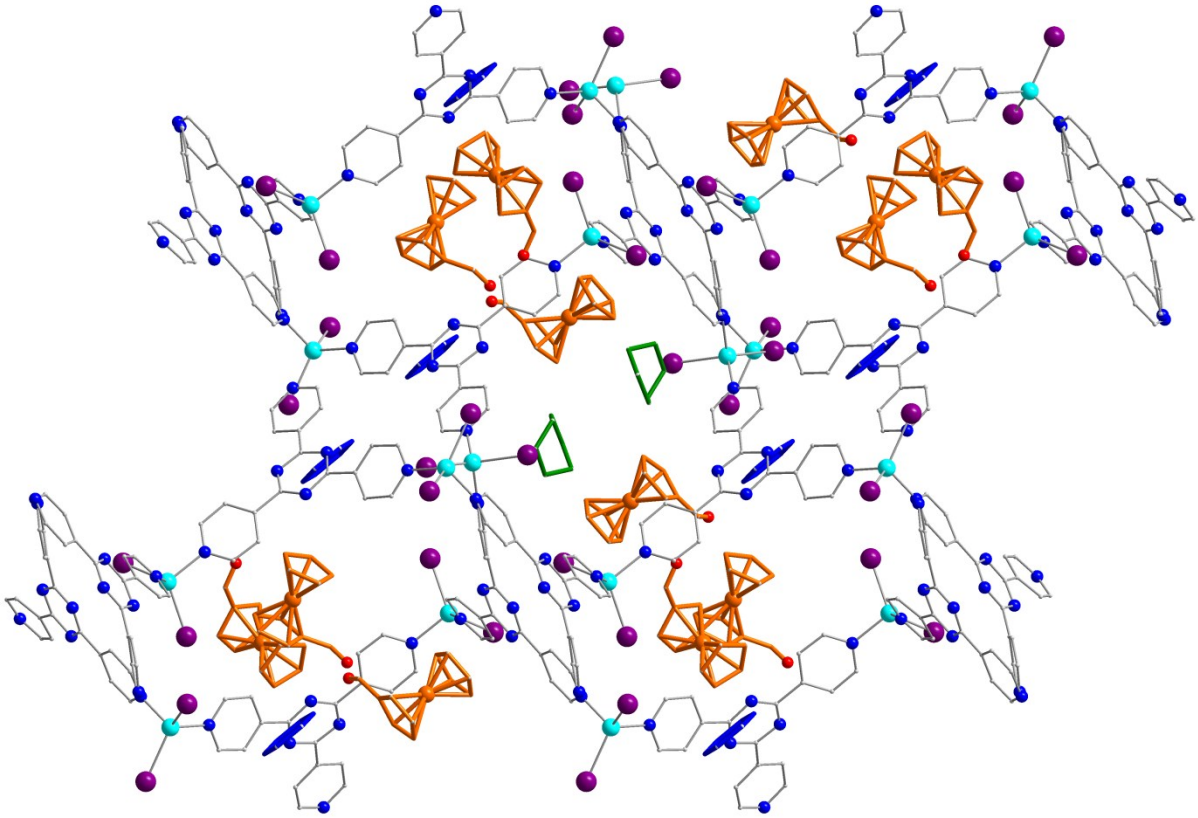

Fig. S4 Packing arrangement of **3** along the *b*-axis, depicting the ferrocene carboxaldehyde guests (orange), and the benzene (blue) and cyclohexane (green) solvent molecules. Hydrogen atoms and positional disorder are omitted for clarity.

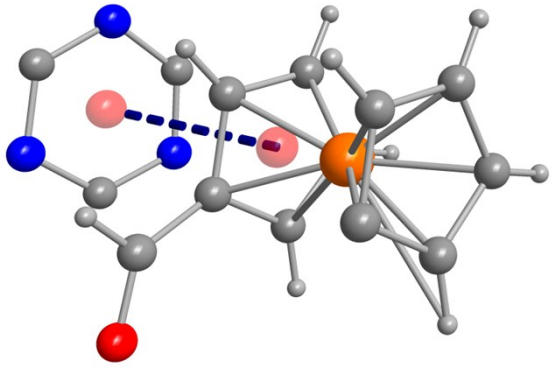

Fig. S5 Face-to-face $\pi\cdots\pi$ stacking interactions between the ferrocene carboxaldehyde guest and the triazine ring of TPT in **3**. Transparent red spheres represent the respective ring centroids. Colour code: orange (Fe), blue (N), gray (C), white (H). red (O).

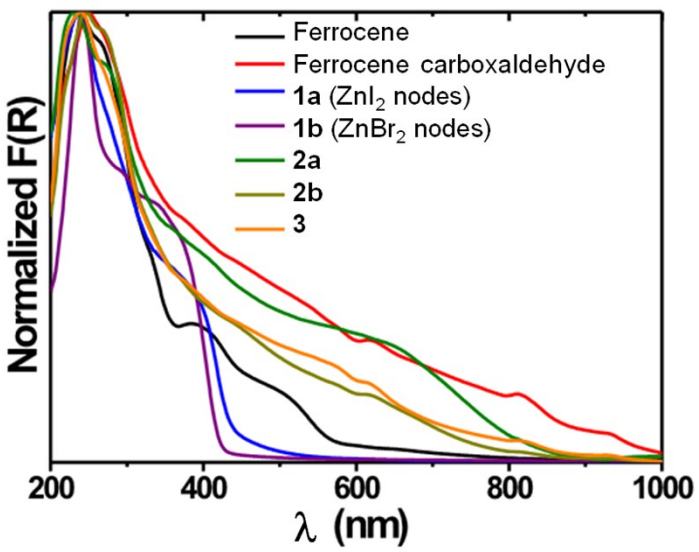

Fig. S6 Normalized Kubelka-Munk spectra of the guest molecules, starting MOFs, and the inclusion compounds.

The diffuse reflectance spectra of both starting MOFs, built from nodes of zinc iodide or zinc bromide, each contain an intense high energy band, accompanied by a shoulder at lower energies slightly above the UV region. The shoulders are likely Laporte forbidden d-d transitions, which occur within the HOMO-LUMO energy gap. While the shoulders in the UV range arise from the $e_{2g} \rightarrow e^*_{1g}$ transition, those in the visible region are due to $a'_{1g} \rightarrow e^*_{1g}$ transition. The intense band in the UV region can be attributed to a charge-transfer arising from the $e_{1u} \rightarrow e^*_{1g}$ transition, which is both spin and Laporte allowed, and thus has a much higher intensity than the d-d transitions. This charge transfer occurs from an e_{1u} orbital, which is more ligand in nature, to a e^*_{1g} orbital that is more metal in nature, and hence would be classified as a ligand-to-metal charge transfer (LMCT).

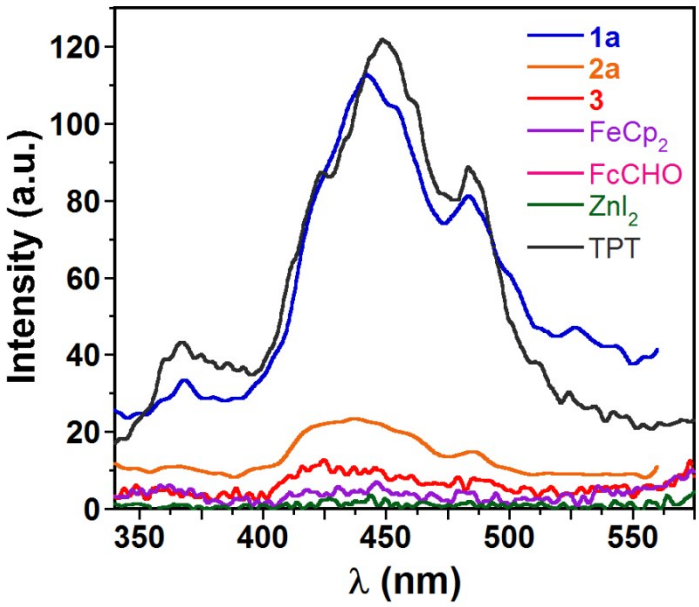

Fig. S7 Solid-state photoluminescence spectra of **1a**, **2a** and **3**, along with the starting materials.

Table S1 Summary of the crystal structure data and refinement for compounds **1a**, **1b**, **2a**, **2b** and **3**.

Complex	**1a**[2]	**1b**[7]	**2a**	**2b**	**3**
Formula	$C_{54}H_{39}I_6N_{15}O_{6.25}Zn_3$	$C_{54}Br6N_{14}O_6Zn_3$	$C_{122}H_{121}Fe_2I_{12}N_{25}O_2Zn_6$	$C_{66.31}H_{71.37}Br_6FeN_{12.46}O_{0.93}Zn_3$	$C_{151}H_{121}Fe_5I_{12}N_{24}O_5Zn_6$
FW, g mol^{-1}	1955.51	1630.29	3996.15	1789.18	4545.98
Crystal system	triclinic	monoclinic	monoclinic	monoclinic	monoclinic
Space group	*P*–1	*C*2/*c*	*C*2/*c*	*C*2/*c*	*C*2/*c*
T, K	193(2)	300	200(2)	150(2)	150(2)
a, Å	14.297(3)	35.218(2)	35.0063(17)	34.1904(4)	38.059(5)
b, Å	17.164(3)	14.6836(7)	15.0958(7)	14.67836(15)	14.2182(11)
c, Å	27.333(5)	30.951(2)	30.2162(15)	30.1683(4)	34.848(6)
α, °	89.970(5)	90	90	90	90
β, °	77.104(4)	103.036(3)	102.0881(19)	101.7441(13)	110.753(16)
γ, °	74.591(4)	90	90	90	90
V, Å^3	6291(2)	15593(9)	15 613.6(13)	14 823.3(3)	17 634(4)
Z	4	8	4	8	4
ρ_{calcd}, g cm^{-3}	2.065		1.700	1.603	1.717
μ (Mo, Kα), mm^{-1}	4.139		3.508	4.434	3.353
reflns collected	21 852		14 326	13 771	15 898
R_1, wR_2 (I > 2 σ (*I*))[a]	0.1194, 0.2720		0.0633, 0.1591	0.0503, 0.1336	0.0492, 0.1184
R_1, wR_2 (all data)	0.3110, 0.3103		0.0739, 0.1655	0.0652, 0.1442	0.0784, 0.1317

[a] $R = R_1 = \| |F_o| - |F_c| / |F_o|$; $wR2 = \{[w(F_o - F_c^2)^2] / [w(F_o^2)^2]\}^{1/2}$; $w = 1/[\sigma_2(F_o^2) + (ap)^2 + bp]$, where $p = [\max(F_o^2, 0) + 2F_c^2]/3$; and $Rw = [w(|F_o| - |F_c|)^2 / w|F_o|^2]^{1/2}$, where $w = 1 / \sigma^2(|F_o|)$.

Table S2 Select bond distances of ferrocene in **2a** and CH···π interactions in a pure ferrocene crystal.

Fe–C bonds (Å)					
Fe61–C62	2.05	Fe61–C66	2.05	Fe61–C70	2.06
Fe61–C63	2.04	Fe61–C67	2.00	Fe61–C71	2.02
Fe61–C64	2.02	Fe61–C68	2.04		
Fe61–C65	2.02	Fe61–C69	2.07		
***π*···*π* interactions in 2a (as defined in Fig. S1 top)**					
1 (Å)		2 (Å)	3 (Å)	α (°)	β (°)
5.45		3.99	3.41	118.32	144.98
***π*···*π* interactions in a pure ferrocene crystal (as defined in Fig. S1 bottom)**					
1 (Å)		2 (Å)	3 (Å)	α (°)	β (°)
4.81		3.59	3.03	112.60	141.16

Table S3 Select bond distances of ferrocene in **2b**.

Fe–C bonds (Å)					
Fe61–C62	2.03	Fe61–C66	2.03	Fe61–C70	2.02
Fe61–C63	2.00	Fe61–C67	2.04	Fe61–C71	2.04
Fe61–C64	2.01	Fe61–C68	2.06		
Fe61–C65	2.02	Fe61–C69	2.03		
***π*···*π* interactions in 2b (as defined in Fig. S1)**					
1 (Å)		2 (Å)	3 (Å)	α (°)	β (°)
5.38		4.01	3.28	115.49	148.83

References

1. M.-X. Li, Z.-X. Miao, M. Shao, S.-W. Liang and S.-R. Zhu, *Inorg. Chem.*, 2008, **47**, 4481–4489.

2. K. Biradha and M. Fujita, *Angew. Chem., Int. Ed.*, 2002, **41**, 3392–3395.

3. Y. Inokuma, S. Yoshioka, J. Ariyoshi, T. Arai and M. Fujita, *Nat. Protoc.*, 2014, **9**, 246–252.

4. *APEX Software Suite v. 2010*, Bruker AXS, Madison, WI, 2005.

5. G. M. Sheldrick, *Acta Cryst.*, 2008, **A64**, 112–122.

6. Rigaku Oxford Diffraction, (2014), CrysAlisPro Software system, version 1.171.37.31, Rigaku Corporation, Oxford, UK.

7. M. Kawano, T. Haneda, D. Hashizume, F. Izumi and M. Fujita, *Angew. Chem., Int. Ed.*, 2008, **47**, 1269–1271.